Half-auxeticity and anisotropic transport in Pd decorated two-dimensional boron sheets

Fengxian Ma[1,#], Yalong Jiao[2,#,*], Weikang Wu[3], Ying Liu[1], Shengyuan A. Yang[3,*], Thomas Heine[2,4,5*]

[1]College of Physics, Hebei Key Laborotory of Photophysics Research and Application, Hebei Normal University, 050024 Shijiazhuang, China

[2]Faculty for Chemistry and Food Chemistry, TU Dresden, Bergstraße 66c, 01069 Dresden, Germany

[3]Research Laboratory for Quantum Materials, Singapore University of Technology and Design, 487372 Singapore, Singapore

[4]Helmholtz-Center Dresden Rossendorf, Institute of Resource Ecology, Leipzig Research Branch, 04316 Leipzig, Germany

[5]Department of Chemistry, Yonsei University, 03722 Seoul, Korea

ABSTRACT

If one strains a material along a direction, most materials shrink normal to that direction. Similarly, if you compress the material, it will expand in the direction orthogonal to the pressure. Few materials, those of negative Poisson ratio, show the opposite behavior. Here, we show an unprecedented feature, a material that expands normal to the direction of force regardless if it is strained or compressed. Such behavior, called half-auxeticity, has been found for a borophene sheet stabilized by decorating Pd atoms. Herein, we explore Pd-decorated borophene, identify three stable phases of which one has this peculiar property of half auxeticity. After carefully analyzing stability, mechanical and electronic properties we explore the origin of this very uncommon behavior.

KEYWORDS

two-dimensional materials, auxetic materials, borophene, buckling structure, first-principle calculations

INTRODUCTION

Among a number of synthetic two-dimensional (2D) flatlands, 2D boron-based materials have sparked great scientific interests in recent research[1,2] due to their unique characteristics including structural polymorphism,[3] optical transparency[4] and versatile band structure features.[5,6] However, the trivalent outer shell of boron cannot completely occupy the in-plane sp^2 bonding state, making their structures fluxional[7] and the synthesis of 2D borophene extremely relies on the metal substrates to compensate the boron's electron-deficiency. To achieve free-standing boron sheets, embedding metal atoms that can donate electrons to the boron frameworks has been considered as an effective strategy. Consequently, some metal-boron monolayers including MgB_2,[8] BeB_2,[9] FeB_2,[10] FeB_6,,[11] MnB,[12] TiB_2[13] and TiB_4[14] have been designed and found to possess novel features including planar hypercoordination, Dirac cones and high Curie temperature.[10,12,14] With many intriguing chemical and physical properties, new 2D metal-boron compounds are expected to have important application potential for nanomechanics and nanoelectronics.

2D materials usually demonstrate excellent mechanical properties, often superior than their three- dimensional (3D) counterparts.[15] They are flexible and can sustain ultra-high critical strains. In recent years, 2D materials with negative Poisson's ratio (NPR) have drawn great attention due to their unconventional lattice response under compression or tension. [16-19] Poisson's ratio $\nu = -\varepsilon_{\text{trans}}/\varepsilon_{\text{axial}}$ is the negative ratio between the strain along the transverse direction $\varepsilon_{\text{trans}}$ in response to an applied uniaxial strain $\varepsilon_{\text{axial}}$. From the daily life experience, most materials would naturally contract in the transverse direction when it is stretched along the longitudinal direction, namely, they have a positive Poisson's ratio (PPR). In contrast, materials with NPR, also known as auxetic materials, would exhibit the rather counterintuitive behavior: they would expand (contract) laterally when a longitudinal tensile (compressive) strain applied. As a result, such materials typically have enhanced toughness, indentation resistance and shear resistance.[20] With these exotic properties, auxetic materials display great potentials in aerospace, biomedicine, military defense and electronics.[21-23] However, compared with 3D bulks, 2D auxetic materials are still rare. Currently, the reported 2D materials with NPR can be classified into three groups, i.e. in-plane NPR (the NPR exists in $\pm x$ or $\pm y$ or other directions within the plane, e.g. penta-graphene),[24] out-of-plane NPR (the NPR exists in $\pm z$ direction, e.g. black phosphorus)[16] and bidirectional NPR (the NPR exists both in-plane and out-of-plane, e.g. Ag_2S, borophene).[25,26] Considering their enhanced mechanical performances and fascinating applications, it is interesting to explore whether there would exist additional auxetic 2D materials, or even new auxeticity types within the class of 2D materials.

In this work, we perform a systematic structure search of palladium borides PdB_n (n=2,3,4) sheets by using first-principles calculations combined with particle swarm optimization (PSO) algorithm[27,28] (see the details in the SI) and revealed a novel NPR material with desirable mechanical and electronic properties. The 2D boron sheets were incorporated with Pd atoms because: It is a transition metal widely used in electronics (as electrodes)[29] and catalysis;[30] it can efficiently donate electrons to boron, and its 2D nanostructures are expected to be well stabilized in experiment;[31] and it has the lowest melting point among the platinum group metals,[32] which could facilitate the experimental synthesis. Finally, three low-energy Pd-B monolayers, one of PdB_4, and two of PdB_2 (PdB_2-I and PdB_2-II) stoichiometries, were discovered in this work. Importantly, the PdB_4 monolayer displays a so-far undiscovered auxetic phenomenon: along one crystal axis, the Poisson's ratio is negative for tensile strains, but becomes positive for compressive strains. As the NPR here occurs only for half of the strain parameter range, we term the effect as "half auxeticity". To our knowledge, such phenomenon has not been reported before, and it renders PdB_4 as an attractive material with potential applications in nanomechanics. Although excellent electronic properties such as high carrier mobilities (~$10^3\ cm^2 \cdot s^{-1} \cdot V^{-1}$ for the semiconducting PdB_2-I sheet) or Dirac loop (for the metallic PdB_2-II sheet) can be found in the PdB_2 monolayers (Fig. 1b and 1c), they are excluded in the following discussion due to their less interesting PPR nature. Nonetheless, as these phases are both thermodynamically stable with formation energies of -105 and -3 meV/atom, respectively, and are very likely to occur when decorating borophene, we discuss their stabilities, structural, electronic and optical properties in detail in the supporting information (Fig. S1-S7).

RESULTS AND DISCUSSION

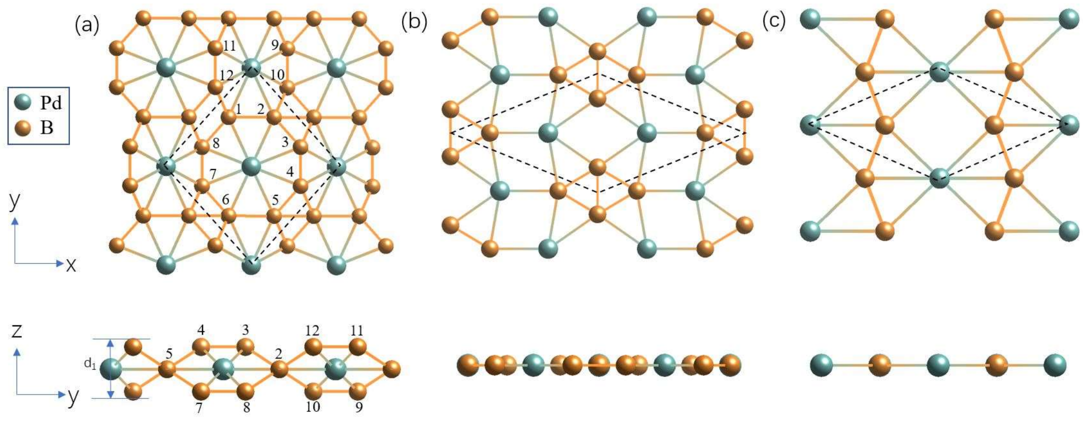

Figure 1. Top and side view of (a) PdB_4, (b) PdB_2-I (c) PdB_2-II monolayers. The dashed frame represents the primitive cell for each structure.

Structure of the PdB_4 monolayer. As shown in Fig. 1a, the B atoms in PdB_4 monolayer form a network composed of 4-membered and 8-membered rings, and more interestingly, each Pd atom is octacoordinated to B atoms, forming Pd-B_8 wheel-like structural motifs.

Such peculiar hypercoordinated structures with B have been attracting great interest for a long time, originally found in molecules/clusters[33-36] and most recently extended to periodic 2D systems.[11,14] The PdB_4 phase crystallizes in the C2/M space group with in-plane anisotropy. More importantly, the structure is not completely planar, but is corrugated with a thickness (d_1) of 1.61 Å. As indicated in Fig. 1a, in each unit cell, four out of the eight B atoms are moved out of the 2D plane formed by other atoms, two shifted above (atom 7, 8) and two shifted down (atom 3, 4). The corrugation significantly stabilizes the 2D sheet by 73.5 meV/atom, indicating the robustness of the buckled geometry. From the Bader charge analysis we find a sizable charge transfer from the Pd (0.22 e per atom) to boron atoms. According to the analysis by Pu et al., [36] in a planar configuration, B_8 ring can only enclose smaller 3d elements, such as Mn, Fe, and Co. Pd is a 4d element with larger radius than 3d. Therefore, the observed buckling is consistent with the previous analysis, and is an intrinsic feature for the hypercoordinated Pd-B_8 wheel structure. As we shall see, the hypercoordination and the buckling play crucial roles in generating the half auxetic effect in PdB_4.

Stability of the PdB_4 monolayer. To access the experimental feasibility to grow the predicted PdB_4 layer, we first evaluated the thermodynamic stability by calculating the formation energy. We define the formation energy per atom E_f with respect to borophene and solid palladium: $E_f = [E(PdB_n) - xE(Pd) - yE(B)]/(x+y)$, where $E(PdB_4)$, $E(Pd)$, and $E(B)$ are the energy of the monolayer, the energy per atom of the solid Pd, and the energy of borophene monolayer,[1] respectively, thus to experimentally available phases of the constituting elements. The estimated E_f for PdB_4 is -42.0 meV/atom, indicating that it is a thermodynamically stable Pd-B phase, even more stable than aggregated Pd clusters at the borophene surface. Based on the elastic stability criteria[37], stable 2D lattices should satisfy: C_{11} , C_{22} , $C_{66} > 0$ & $C_{11} + C_{22} - 2C_{12} > 0$, where C_{ij} are the elastic constants. This criterion is met here, see Table S1 for summarized values.

There are no imaginary frequencies in the phonon dispersion (Fig. S1a), which otherwise shows the typical behavior of a kinetically stable 2D material, with two linear and one parabolic acoustic branches. The highest frequencies of PdB_4 reach up to 1214 cm^{-1} (36.4 THz), which is higher than the highest frequencies found in silicene (580 cm^{-1}),[38] Cu_2Si (420 cm^{-1})[39], MoS_2 monolayers (473 cm^{-1}).[40]. Such high-energy phonons characterize the robust Pd−B and B−B interactions in PdB_4. We further perform AIMD simulation at 300 K to evaluate the thermal stability of the PdB_4 sheet, in which a supercell containing 80 atoms was used. The snapshot taken at the end of 10 ps simulation is presented in Fig. S2a. We find the framework is well preserved as in the original configuration, indicating it is thermally stable.

Electronic properties of the PdB_4 monolayer. PdB_4 monolayer is a semiconductor with an indirect gap of, at the HSE06 hybrid functional level, 1.22 eV. As shown in Fig. 2, the valence band maximum (VBM) for PdB_4 phase is along M-Γ line, while the conduction band minimum (CBM) locates at M point. From the projected density of states (PDOS), it can be found both VBM and CBM of PdB_4 and PdB_2 are contributed by the hybridized Pd-*d* and B-*p* states (Fig. 2b). The partial charge density distributions plotted in Fig. 2c-2d is in consistence with the PDOS results. The carrier (electron or hole) mobility of 2D materials has a great effect on the performance of electronic devices. We thus evaluated the charge transport of PdB_4 based on deformation potential (DP) theory. [41] The details for the carrier mobility (μ) results are provided in the SI (Fig. S8 and Table S2). For PdB_4 monolayer, the calculated electron (hole) mobility along y direction is 2270 (1640) $cm^2 \cdot s^{-1} \cdot V^{-1}$, which is much larger than that along x direction (960 (43) $cm^2 \cdot s^{-1} \cdot V^{-1}$). This indicates carrier transport is preferred along y direction. Notably, the carrier mobilities for PdB_4 are comparable to that in phosphorene ($\sim 10^4$ $cm^2 \cdot s^{-1} \cdot V^{-1}$)[42], and higher than that of 2D transition metal dichalcogenides such as MoS_2 ($\sim 10^2$ $cm^2 \cdot s^{-1} \cdot V^{-1}$)[43], demonstrating its excellent conductivity.

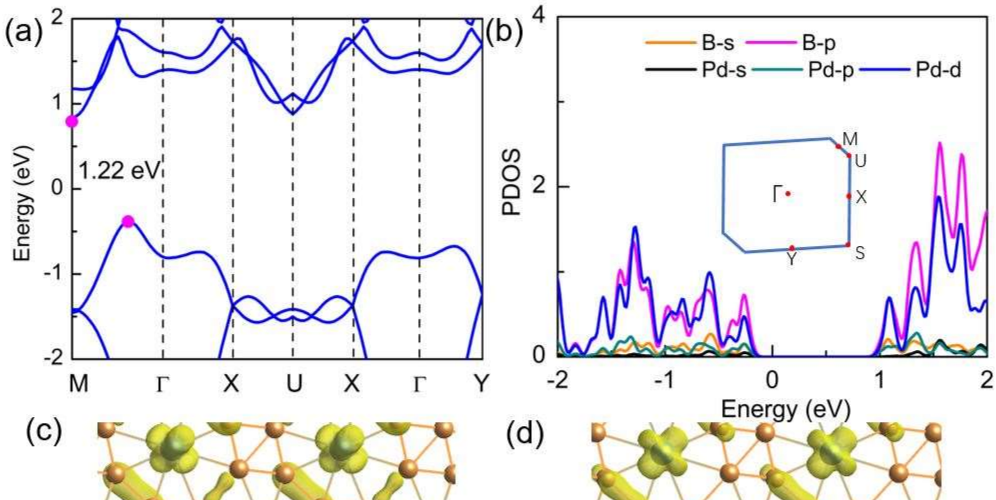

Figure 2. (a) Band structure and (b) PDOS for PdB_4 monolayer. Inset of (b): The Brillouin zone. (c-d) Partial charge density distributions of the VBM and CBM for PdB_4 monolayer. The isosurface is set to be 0.01 eÅ^{-3}.

Strain effect of the PdB_4 monolayer. We then explore the strain effect on the electronic properties PdB_4 monolayer. In Fig. 3, we present the evolution of band edge levels and energy gaps under the strain along x direction. The uniaxial strain is defined as $\varepsilon_i = \frac{l_i - l_{i0}}{l_{i0}} \times 100\%$, where i represents a certain direction such as x, y or z. l_i *and* l_{i0} represent the lattice constant under a certain strain and for a strain-free system, respectively. As the results for the y direction are similar (Fig. S9), they are therefore not displayed here. In the strain range from -6% to +6%, we find the position of CBM drops down to lower energy level when strain increases, while that of CBM shifts up towards the Fermi level. Consequently, the energy gap E_g decreases with the increased strain. To quantify the sensitivity of strain against E_g, we plot the rate of change of E_g ($R(E_g)$)with respect to ε_x, which is defined as the change of bandgap over the change of strain, i.e. $\Delta E_g/\Delta\varepsilon_x$. Results show that in an experimentally available strain of 2%, the absolute value of $R(E_g)$ researches up to ~110 meV/% strain, which is higher than that of single-layer transition metal dichalcogenides such as MoS_2 (45 meV/%)[44], WSe_2 (60-70 meV/%)[45] and $MoSe_2$ (27 meV/%)[46]. The pronounced rate of change indicates electronic properties of PdB_4 monolayer is highly sensitive to the strain engineering and thus exhibits promising application in strain sensors.

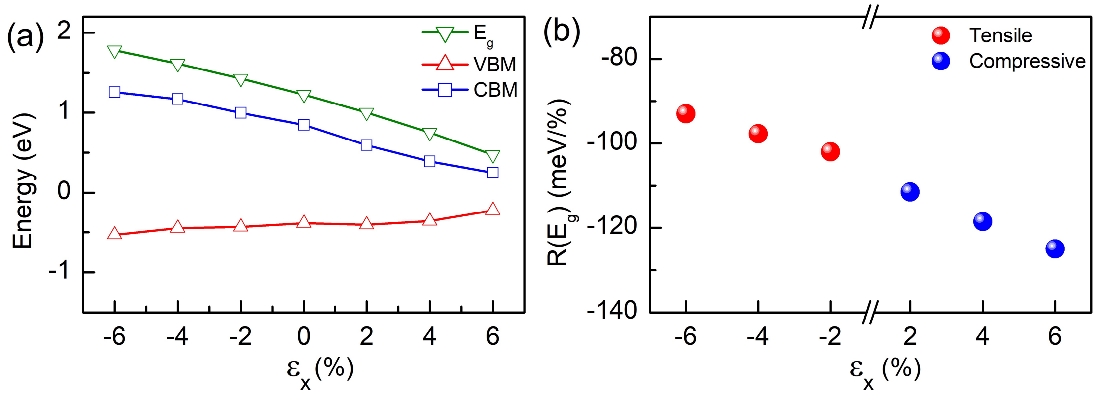

Figure 3. (a) Band edge positions and band gap (E_g) of PdB_4 monolayer under uniaxial strains x. (b) rate of change of bandgap ($R(E_g)$) as a function of uniaxial tensile/compressive strain.

Mechanical properties of the PdB_4 monolayer. The unique geometries in the Pd-B_8 wheels in PdB_4 sheet show fascinating mechanical performance, and it is thus intriguing to explore them in more detail. In the elastic theory, 2D Young's modulus along x and y direction is defined by elastic constants as $Y_x^{2D} = C_{11}C_{22} - C_{12}C_{21}/C_{22}$ and $Y_y^{2D} = C_{11}C_{22} - C_{12}C_{21}/C_{11}$, respectively. The evaluated Y_x^{2D} and Y_y^{2D} are 105.7 and 121.4 GPa·nm for PdB_4, which is mechanically anisotropic. The values are about 32% - 47% of that in 2D MoS_2 (330 GPa·nm)[47], but larger than that of phosphorene (23.0 GPa·nm along armchair and 92.3 GPa·nm along zigzag direction),[48] demonstrating they are flexible materials. The corresponding Poisson's ratios ν, defined as $\nu_x^{2D} = C_{12}/C_{22}$; $\nu_y^{2D} = C_{12}/C_{11}$, is found to be negative for PdB_4 due to the negative C_{12}, indicating it is an auxetic material.

Next, we explore the mechanical properties of PdB_4 monolayer under uniaxial strain. Generally, the strain disturbs the equilibrium state of the structure, thus the total energy of the system will rise (see strain-energy curve in Fig. S10). To provide an overall picture, the resultant strains (including both in-plane and vertical directions) in response to uniaxial deformation ranging from −8% to 8% is plotted by using a rectangular unit cell (Fig. S8a). We notice that our conclusions will not be changed when a primitive cell was used (Fig. S11). From Fig. 4b and 4d， one can see that the layer thickness (strain along *z*) decreases with the increase of the in-plane strain (along *x* and *y*), indicating the out-of-plane Poisson's ratios in PdB_4 sheet are always positive. To explore the in-plane Poisson's ratios, we consider uniaxial deformation of the sheet along *x* and monitor the change along *y*. Figure 4a shows that a nonlinear behavior is observed. By fitting the data to the function $y = -v_1x + v_2x^2 + v_3x^3$, with v_1 defined as the linear Poisson's ratio, we found the value of v_1 is -0.016, which confirms a negative in-plane Poisson's ratio in the *x* direction. This means that a PdB_4 sheet will expand (contract) along *y* when it is stretched (compressed) along *x*, corresponding to the auxetic behavior.

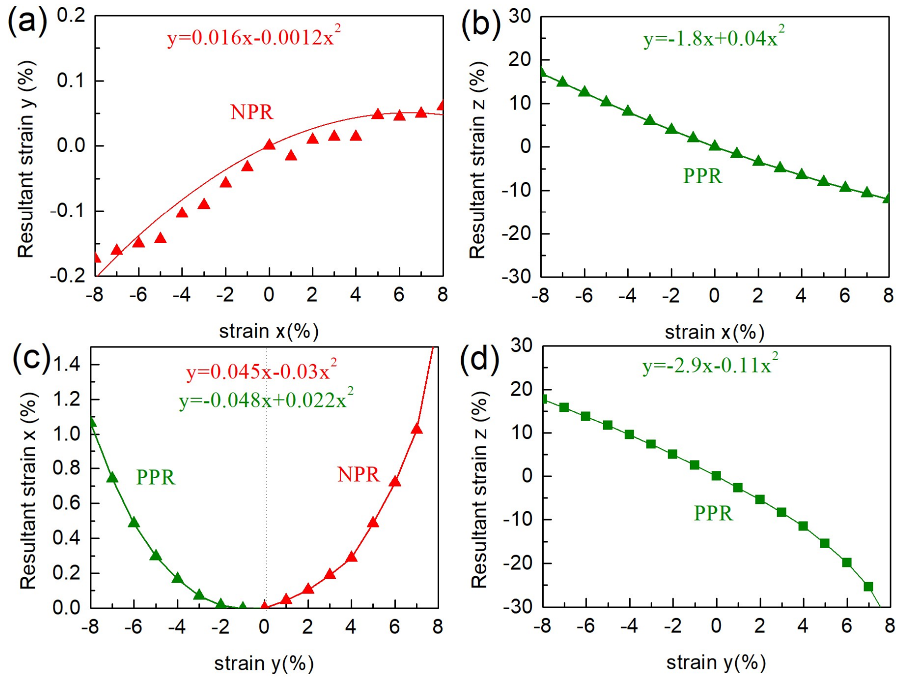

Figure 4. Mechanical response of PdB_4 monolayer under uniaxial strain along (a-b) x- and (c-d) y-directions. In the calculation, a rectangular cell was used. Data are fitted to the function $y = -v_1x + v_2x^2 + v_3x^3$.

Remarkably, the in-plane Poisson's ratio in the *y* direction shows a distinct behavior. Under tensile strain along *y*, the lateral dimension along *x* will expand, as indicated by the red data points in Fig. 4c. This gives a negative Poisson's ratio. The fitted v_1 is -0.045, which is comparable to the reported auxetic materials, such as single-layer black phosphorus

(-0.027)[16], borophane (-0.053),[26] Be_5C_2 monolayer (-0.041)[18] and penta-graphene (−0.068)[17]. Normally, an auxetic material would contract under a compressive strain, i.e., the Poisson's ratio maintains the same sign for negative strain (although its absolute value may change). Surprisingly, for PdB_4, under a compressive y-strain, the lattice size along x displays a response opposite to our expectation, i.e. an increasing trend, indicating a positive Poisson's ratio (v_1=0.048) for this case (as indicated by the olive data points in Fig. 4c). In other words, the Poisson's ratio has a sign change at the equilibrium, between positive and negative strains along y direction. We call this behavior the half-auxetic effect. With this effect, PdB_4 exhibits the peculiar behavior that it always expands along x whenever it is strained along y, regardless of whether this strain is tensile or compressive.

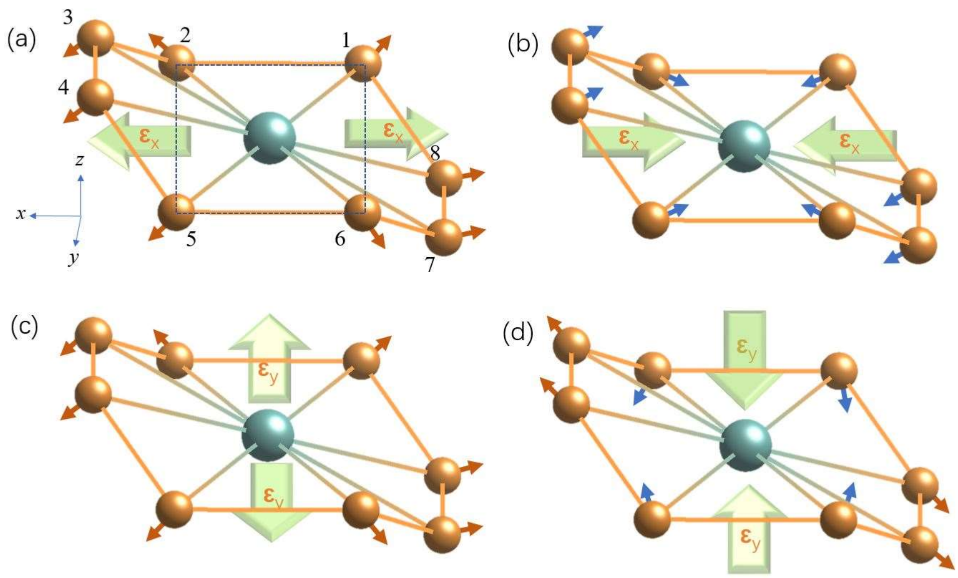

Figure 5. The structural evolution of the Pd-B_8 wheel of PdB_4 monolayer under uniaxial tensile/compressive strain along (a-b) x and (c-d) y direction, respectively. Transparent green arrows represent strain directions. Solid orange/blue arrows display the atoms move outward/inward. Atom 1, 2, 5 and 6 are within the *x-y (z=0)* plane (blue dashed frame).

Origin of the auxetic properties of PdB_4 monolayer. The auxetic properties of PdB_4 monolayer are intimately connected with the hypercoordinated Pd-B_8 wheel motif in its structure. As shown in Fig. 1, the Pd-B_8 wheel has an intrinsic out-of-plane buckling. To visualize this feature more clearly, we plot an enlarged view of the Pd-B_8 wheel in Fig. 5. Here, the Pd atom and B atoms labeled 1, 2, 5, and 6 are within the same 2D *x-y* plane (referred to as the z=0 plane), B 3 and 4 are above this plane, whereas B 7 and 8 are below the plane. First, consider the uniaxial strain applied along the x direction, for which the movement of the atoms is illustrated in Fig. 5a. One observes that when the wheel is stretched along x, the four out-of-plane B atoms will naturally move towards the z=0 plane. This movement will push out B 1, 2, 5 and 6 along y, because the bond lengths between the B sites should be kept more or less unchanged due to the strong interatomic forces. Conversely, when the wheel is compressed along *x* (Fig. 5b), the four out-of-plane B will move further away from the *z*=0 plane, and the four in-plane B will then shift towards Pd. This explains the observed auxetic behavior for strains along *x*. Under a tensile strain along *y* direction (Fig. 5c), on the other hand, the four in-plane B atoms are stretched away from the center of the wheel. Due to the bonding between B sites, the four out-of-plane B move towards the *z*=0 plane, i.e., the thickness of the sheet naturally shrinks due to the in-plane stretch. Meanwhile, these out-of-plane B also have strong bonding with the central Pd, which maintains a more or less unchanged bond length (between Pd and B 3, 4, 7, 8) in this process. This leads to the observed expansion along *x*. Note that the reduction of thickness in this case is remarkably high, e.g. it reaches more than 30% under +8% strain along *y*. This explains the observed sizable negative Poisson's ratio. Finally, consider the compressive strain along *y*. The in-plane B 1, 2, 5 and 6 are moved inward under strain (see Fig. 5d). For the out-of-plane B 3, 4, 7, and 8, under the joint forces from the in-plane B and Pd, their natural choices are (1) move further away from the *z*=0 plane and (2) move outward along *x*. From our above discussion, the movement (1) may lead to a shrink along *x*, but it turns out that this tendency is subdominant here and is surpassed by the movement (2). This results in the observed positive Poisson's ratio for compressive strains along *y*. From the above analysis, it is clear that the unusual half-auxetic effect in PdB_4 is a consequence of the special hypercoordinated Pd-B_8 wheel structure.

CONCLUSION

Our study of the 2D palladium borides provides a concrete example for exploring transition-metal borides as promising material systems with distinct properties. By searching for low-energy 2D Pd-B compounds, we identified three monolayers, namely one PdB_4 and two PdB_2 sheet possessing high chemical, dynamical and mechanical stabilities. In particular, single-layer PdB_4 consisting of buckled Pd-B_8 wheels is a hypercoordinated structure. Arising from its unique structural configuration, PdB_4 sheet exhibits a novel auxetic property, in which a NPR to PPR transition can be found when changing the sign of strain. Such a half-auxetic feature has not yet been reported in 2D materials. Additionally, the PdB_4 monolayer show high carrier motilities and the band gap of PdB_4 sheet is highly tunable by the strain effect. The fascinating properties, including half-auxeticity, ultrahigh mobilities and strain-sensitive bandgaps make PdB_4 monolayer an ideal integrated platform for nanoscale device applications.

ASSOCIATED CONTENT

Supporting Information

The Supporting Information is available free of charge.

Supplementary results including computational details of this work, the phonon spectrum, AIMD simulations, elastic constants and structural information for all predicted structures, band structures, PDOS, partial charge density distributions and light absorbance for the PdB_2 monolayers, electronic property and elastic energy of PdB_4 monolayer under strain effect.

AUTHOR INFORMATION

Corresponding Authors

*E-mail: yalong.jiao@mailbox.tu-dresden.de (Y.J.)
*E-mail: shengyuan_yang@sutd.edu.sg (S.A.Y.)
*E-mail: thomas.heine@tu-dresden.de (T.H.)

Notes

# These authors contributed equally. The authors declare no competing financial interest.

ACKNOWLEDGMENT

F.M. acknowledges the support from the National Natural Science Foundation of China (Grant No. 11847017 and 11904077), Science Foundation of Hebei Normal University (Grant No. L2019B09) and financial support program from Hebei Province (Grant No. E2019050018). Y. J. appreciates the funding from the Alexander von Humboldt-Foundation. S. A. Y. is supported by the Singapore MOE AcRF Tier 2 (Grant No. MOE2019-T2-1-001).

REFERENCES

(1) Mannix, A. J.; Zhou, X.-F.; Kiraly, B.; Wood, J. D.; Alducin, D.; Myers, B. D.; Liu, X.; Fisher, B. L.; Santiago, U.; Guest, J. R.; Yacaman, M. J.; Ponce, A.; Oganov, A. R.; Hersam, M. C.; Guisinger, N. P. Synthesis of borophenes: Anisotropic, two-dimensional boron polymorphs. *Science* **2015**, *350*, 1513-1516.

(2) Feng, B.; Zhang, J.; Zhong, Q.; Li, W.; Li, S.; Li, H.; Cheng, P.; Meng, S.; Chen, L.; Wu, K. Experimental realization of two-dimensional boron sheets. *Nature Chemistry* **2016**, *8*, 563-568.

(3) Wu, X.; Dai, J.; Zhao, Y.; Zhuo, Z.; Yang, J.; Zeng, X. C. Two-dimensional boron monolayer sheets. *ACS nano* **2012**, *6*, 7443-7453.

(4) Adamska, L.; Sadasivam, S.; Foley IV, J. J.; Darancet, P.; Sharifzadeh, S. First-principles investigation of borophene as a monolayer transparent conductor. *The Journal of Physical Chemistry C* **2018**, *122*, 4037-4045.

(5) Feng, B.; Sugino, O.; Liu, R.-Y.; Zhang, J.; Yukawa, R.; Kawamura, M.; Iimori, T.; Kim, H.; Hasegawa, Y.; Li, H.; Chen, L.; Wu, K.; Kumigashira, H.; Komori, F.; Chiang, T.-C.; Meng, S.; Matsuda, I. Dirac Fermions in Borophene. *Physical Review Letters* **2017**, *118*, 096401.

(6) Ma, F.; Jiao, Y.; Gao, G.; Gu, Y.; Bilic, A.; Chen, Z.; Du, A. Graphene-like Two-Dimensional Ionic Boron with Double Dirac Cones at Ambient Condition. *Nano Letters* **2016**, *16*, 3022-3028.

(7) Jalife, S.; Liu, L.; Pan, S.; Cabellos, J. L.; Osorio, E.; Lu, C.; Heine, T.; Donald, K. J.; Merino, G.

Dynamical behavior of boron clusters. *Nanoscale* **2016**, *8*, 17639-17644.

(8) Tang, H.; Ismail-Beigi, S. First-principles study of boron sheets and nanotubes. *Physical Review B* **2010**, *82*, 115412.

(9) Zhang, P.; Crespi, V. H. Theory of ${\mathrm{B}}_{\mathrm{2}}\mathrm{O}$ and ${\mathrm{B}\mathrm{e}\mathrm{B}}_{2}$ Nanotubes: New Semiconductors and Metals in One Dimension. *Physical Review Letters* **2002**, *89*, 056403.

(10) Zhang, H.; Li, Y.; Hou, J.; Du, A.; Chen, Z. Dirac State in the FeB2 Monolayer with Graphene-Like Boron Sheet. *Nano Letters* **2016**, *16*, 6124-6129.

(11) Zhang, H.; Li, Y.; Hou, J.; Tu, K.; Chen, Z. FeB_6 Monolayers: The Graphene-like Material with Hypercoordinate Transition Metal. *Journal of the American Chemical Society* **2016**, *138*, 5644-5651.

(12) Jiang, Z.; Wang, P.; Jiang, X.; Zhao, J. MBene (MnB): a new type of 2D metallic ferromagnet with high Curie temperature. *Nanoscale Horizons* **2018**, *3*, 335-341.

(13) Zhang, L. Z.; Wang, Z. F.; Du, S. X.; Gao, H. J.; Liu, F. Prediction of a Dirac state in monolayer ${\mathrm{TiB}}_{2}$. *Physical Review B* **2014**, *90*, 161402.

(14) Qu, X.; Yang, J.; Wang, Y.; Lv, J.; Chen, Z.; Ma, Y. A two-dimensional TiB_4 monolayer exhibits planar octacoordinate Ti. *Nanoscale* **2017**, *9*, 17983-17990.

(15) Akinwande, D.; Brennan, C. J.; Bunch, J. S.; Egberts, P.; Felts, J. R.; Gao, H.; Huang, R.; Kim, J.-S.; Li, T.; Li, Y. J. E. M. L. A review on mechanics and mechanical properties of 2D materials—Graphene and beyond. *Extreme Mechanics Letters* **2017**, *13*, 42-77.

(16) Jiang, J.-W.; Park, H. S. Negative poisson's ratio in single-layer black phosphorus. *Nature Communications* **2014**, *5*, 4727.

(17) Zhang, S.; Zhou, J.; Wang, Q.; Chen, X.; Kawazoe, Y.; Jena, P. Penta-graphene: A new carbon allotrope. *Proceedings of the National Academy of Sciences* **2015**, *112*, 2372-2377.

(18) Wang, Y.; Li, F.; Li, Y.; Chen, Z. Semi-metallic Be_5C_2 monolayer global minimum with quasi-planar pentacoordinate carbons and negative Poisson's ratio. *Nature Communications* **2016**, *7*, 11488.

(19) Peng, R.; Ma, Y.; Wu, Q.; Huang, B.; Dai, Y. Two-dimensional materials with intrinsic auxeticity: progress and perspectives. *Nanoscale* **2019**, *11*, 11413-11428.

(20) Fang, R.; Cui, X.; Stampfl, C.; Ringer, S. P.; Zheng, R. Negative Poisson's ratio in 2D life-boat structured crystals. *Nanoscale Advances* **2019**, *1*, 1117-1123.

(21) Scarpa, F.; Yates, J.; Ciffo, L.; Patsias, S. J. P. o. t. I. o. M. E., Part C: Journal of Mechanical Engineering Science. Dynamic crushing of auxetic open-cell polyurethane foam. **2002**, *216*, 1153-1156.

(22) Friis, E. A.; Lakes, R. S.; Park, J. B. Negative Poisson's ratio polymeric and metallic foams. *Journal of Materials Science* **1988**, *23*, 4406-4414.

(23) Alderson, A.; Alderson, K. J. P. o. t. I. o. M. E., Part G: Journal of Aerospace Engineering. Auxetic materials. **2007**, *221*, 565-575.

(24) Zhang, S.; Zhou, J.; Wang, Q.; Chen, X.; Kawazoe, Y.; Jena, P. Penta-graphene: A new carbon allotrope. **2015**, *112*, 2372-2377.

(25) Peng, R.; Ma, Y.; He, Z.; Huang, B.; Kou, L.; Dai, Y. Single-Layer Ag2S: A Two-Dimensional Bidirectional Auxetic Semiconductor. *Nano Letters* **2019**, *19*, 1227-1233.

(26) Kou, L.; Ma, Y.; Tang, C.; Sun, Z.; Du, A.; Chen, C. Auxetic and Ferroelastic Borophane: A Novel 2D Material with Negative Possion's Ratio and Switchable Dirac Transport Channels. *Nano Letters* **2016**, *16*, 7910-7914.

(27) Wang, Y.; Lv, J.; Zhu, L.; Ma, Y. Crystal structure prediction via particle-swarm optimization. *Phys. Rev. B* **2010**, *82*, 094116.

(28) Wang, Y.; Lv, J.; Zhu, L.; Ma, Y. CALYPSO: A method for crystal structure prediction. *Comput. Phys. Commun.* **2012**, *183*, 2063-2070.

(29) Wang, J.-Y.; Zhang, H.-X.; Jiang, K.; Cai, W.-B. From HCOOH to CO at Pd Electrodes: A Surface-Enhanced Infrared Spectroscopy Study. *Journal of the American Chemical Society* **2011**, *133*, 14876-14879.

(30) Nishihata, Y.; Mizuki, J.; Akao, T.; Tanaka, H.; Uenishi, M.; Kimura, M.; Okamoto, T.; Hamada, N. Self-regeneration of a Pd-perovskite catalyst for automotive emissions control. *Nature* **2002**, *418*, 164-167.

(31) Noh, J.-S.; Lee, J. M.; Lee, W. Low-dimensional palladium nanostructures for fast and reliable hydrogen gas detection. *Sensors* **2011**, *11*, 825-851.

(32) Rao, C. R. K.; Trivedi, D. C. Chemical and electrochemical depositions of platinum group metals and their applications. *Coordination Chemistry Reviews* **2005**, *249*, 613-631.

(33) Romanescu, C.; Galeev, T. R.; Li, W.-L.; Boldyrev, A. I.; Wang, L.-S. Transition-Metal-Centered Monocyclic Boron Wheel Clusters (M©Bn): A New Class of Aromatic Borometallic Compounds. *Accounts of Chemical Research* **2013**, *46*, 350-358.

(34) Islas, R.; Heine, T.; Ito, K.; Schleyer, P. v. R.; Merino, G. Boron Rings Enclosing Planar Hypercoordinate Group 14 Elements. *Journal of the American Chemical Society* **2007**, *129*, 14767-14774.

(35) Ito, K.; Pu, Z.; Li, Q.-S.; Schleyer, P. v. R. Cyclic Boron Clusters Enclosing Planar Hypercoordinate Cobalt, Iron, and Nickel. *Inorganic Chemistry* **2008**, *47*, 10906-10910.

(36) Pu, Z.; Ito, K.; Schleyer, P. v. R.; Li, Q.-S. Planar Hepta-, Octa-, Nona-, and Decacoordinate First Row d-Block Metals Enclosed by Boron Rings. *Inorganic Chemistry* **2009**, *48*, 10679-10686.

(37) Wu, Z.-j.; Zhao, E.-j.; Xiang, H.-p.; Hao, X.-f.; Liu, X.-j.; Meng, J. Crystal structures and elastic properties of superhard IrN_2 and IrN_3 from first principles. *Physical Review B* **2007**, *76*, 054115.

(38) Cahangirov, S.; Topsakal, M.; Aktürk, E.; Şahin, H.; Ciraci, S. Two-and one-dimensional honeycomb structures of silicon and germanium. *Physical Review Letters* **2009**, *102*, 236804.

(39) Yang, L.-M.; Bačić, V.; Popov, I. A.; Boldyrev, A. I.; Heine, T.; Frauenheim, T.; Ganz, E. Two-Dimensional Cu_2Si Monolayer with Planar Hexacoordinate Copper and Silicon Bonding. *Journal of the American Chemical Society* **2015**, *137*, 2757-2762.

(40) Molina-Sanchez, A.; Wirtz, L. Phonons in single-layer and few-layer MoS_2 and WS_2. *Physical Review B* **2011**, *84*, 155413.

(41) Bardeen, J.; Shockley, W. Deformation Potentials and Mobilities in Non-Polar Crystals. *Physical Review* **1950**, *80*, 72-80.

(42) Qiao, J.; Kong, X.; Hu, Z.-X.; Yang, F.; Ji, W. High-mobility transport anisotropy and linear dichroism in few-layer black phosphorus. *Nature Communications* **2014**, *5*, 4475.

(43) Rawat, A.; Jena, N.; Dimple; De Sarkar, A. A comprehensive study on carrier mobility and artificial photosynthetic properties in group VI B transition metal dichalcogenide monolayers. *Journal of Materials Chemistry A* **2018**, *6*, 8693-8704.

(44) Conley, H. J.; Wang, B.; Ziegler, J. I.; Haglund, R. F.; Pantelides, S. T.; Bolotin, K. I. Bandgap Engineering of Strained Monolayer and Bilayer MoS2. *Nano Letters* **2013**, *13*, 3626-3630.

(45) Desai, S. B.; Seol, G.; Kang, J. S.; Fang, H.; Battaglia, C.; Kapadia, R.; Ager, J. W.; Guo, J.; Javey, A. Strain-Induced Indirect to Direct Bandgap Transition in Multilayer WSe2. *Nano Letters* **2014**, *14*, 4592-4597.

(46) Island, J. O.; Kuc, A.; Diependaal, E. H.; Bratschitsch, R.; van der Zant, H. S. J.; Heine, T.; Castellanos-Gomez, A. Precise and reversible band gap tuning in single-layer MoSe2 by uniaxial strain.

Nanoscale **2016**, *8*, 2589-2593.

(47) Castellanos-Gomez, A.; Poot, M.; Steele, G. A.; van der Zant, H. S. J.; Agraït, N.; Rubio-Bollinger, G. Elastic Properties of Freely Suspended MoS_2 Nanosheets. **2012**, *24*, 772-775.

(48) Wang, L.; Kutana, A.; Zou, X.; Yakobson, B. I. Electro-mechanical anisotropy of phosphorene. *Nanoscale* **2015**, *7*, 9746-9751.

Table of Contents